

Article

Interfacial Behavior of Oligo(Ethylene Glycol) Dendrons Spread Alone and in Combination with a Phospholipid as Langmuir Monolayers at the Air/Water Interface

Da Shi ¹, Dinh-Vu Nguyen ² , Mounir Maaloum ¹, Jean-Louis Gallani ² ,
Delphine Felder-Flesch ² and Marie Pierre Krafft ^{1,*}

¹ Institut Charles Sadron (CNRS), University of Strasbourg, 23 rue du Loess, 67034 Strasbourg CEDEX 2, France; da.shi@ics-cnrs.unistra.fr (D.S.); maaloum@unistra.fr (M.M.)

² Institut de Physique et Chimie des Matériaux de Strasbourg (IPCMS, CNRS), University of Strasbourg, 23 rue du Loess. 67034 Strasbourg CEDEX 2, France; dinh-vu.nguyen@alumni.chimie-paritech.fr (D.-V.N.); gallani@ipcms.unistra.fr (J.-L.G.); delphine.felder@ipcms.unistra.fr (D.F.-F.)

* Correspondence: krafft@unistra.fr; Tel.: +33388414060; Fax: +33388414099

Academic Editor: Richard A Campbell

Received: 18 October 2019; Accepted: 11 November 2019; Published: 14 November 2019



Abstract: Dendrons consisting of two phosphonate functions and three oligo(ethylene glycol) (OEG) chains grafted on a central phenoxyethylcarbonylphenoxy group were synthesized and investigated as Langmuir monolayers at the surface of water. The OEG chain in the *para* position was grafted with a *t*-Bu end-group, a hydrocarbon chain, or a partially fluorinated chain. These dendrons are models of structurally related OEG dendrons that were found to significantly improve the stability of aqueous dispersions of iron oxide nanoparticles when grafted on their surface. Compression isotherms showed that all OEG dendrons formed liquid-expanded Langmuir monolayers at large molecular areas. Further compression led to a transition ascribed to the solubilization of the OEG chains in the aqueous phase. Brewster angle microscopy (BAM) provided evidence that the dendrons fitted with hydrocarbon chains formed liquid-expanded monolayers throughout compression, whilst those fitted with fluorinated end-groups formed crystalline-like domains, even at large molecular areas. Dimyristoylphosphatidylcholine and dendron molecules were partially miscible in monolayers. The deviations to ideality were larger for the dendrons fitted with a fluorocarbon end-group chain than for those fitted with a hydrocarbon chain. Brewster angle microscopy and atomic force microscopy supported the view that the dendrons were ejected from the phospholipid monolayer during the OEG conformational transition and formed crystalline domains on the surface of the monolayer.

Keywords: fluorocarbon; interfacial film; Brewster angle microscopy; atomic force microscopy; molecular recognition

1. Introduction

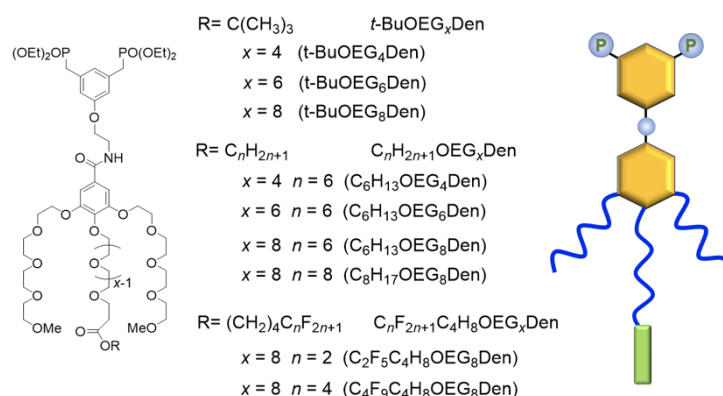
Dendrimers are monodisperse macromolecules with a regular, highly branched, and well defined three-dimensional architecture, which have garnered interest in nanotechnology, materials science, and medicine [1–3]. In particular, they have been used in the synthesis and stabilization of metal nanoparticles used as drug delivery carriers and chemical and biomedical sensors [4]. Dendrons, which are fractional dendrimers, can assemble in solution to form a variety of nano- and microstructures [5,6], and have been found to form stable organized molecular films at the air/water interface [7]. Oligo(ethylene glycol) (OEG) dendrons have been used as efficient coating agents of iron oxide nanoparticles (IONPs) to improve the dispersibility and stability of these nanoparticles in aqueous

solution [8,9]. Poly(ethylene glycol) (PEG) dendron-based phospholipids have been utilized for the preparation of stealth liposomes in biomedical applications [10]. Understanding the behavior of PEG and OEG dendrons is key to the development of interfacial applications [11,12]. The physicochemical properties of dendrons and, in particular, their interfacial behavior, strongly depend on their nature, generation number, and ratio of hydrophilic and hydrophobic parts [13,14]. Langmuir films are an effective tool for studying monolayers of amphiphilic dendrimers or dendrons at the air/water interface, which provide information such as dendron size, shape, and compressibility [11,15]. The Langmuir–Blodgett (LB) technique is commonly used for the fabrication of ordered monolayers by transfer onto solid substrate surfaces. Information about the microstructure of monolayers of dendrimers prepared by the LB technique has been obtained using X-ray, atomic force microscopy (AFM), Brewster angle microscopy (BAM), and neutron reflectivity [14,16–18].

Although numerous studies have reported on the behavior of dendrimers or dendrons at the air/water interface, few investigations have focused on the morphology and orientation of dendrons bearing OEG chains. One study of dendrons fitted with an OEG chain and poly(benzyl ether) (third to fifth generation) showed that stability of the monolayers increased with OEG chain length [7]. The stability of monolayers of OEGylated carbazole dendrons was found to depend mostly on the generation of the hydrophobic part [19]. The interfacial behavior of polyol–polyether dendritic amphiphiles fitted with two hydrocarbon chains has been examined [20], as well as the interactions of these dendrons with dipalmitoylphosphatidylcholine (DPPC) [21]. A compression isotherm and BAM study indicated that dendrons with the highest generation of polyglycerol form denser monolayers, and that they form mutually soluble binary mixtures with the phospholipid.

Here, we investigated the behavior of OEG-based dendrons at the air/water interface, and the behavior of combinations of these dendrons with dimyristoylphosphatidylcholine (DMPC). Our OEG dendrons consisted of a central phenoxyethylcarbamoyl group coupled to a phenyl group onto which three OEG chains were grafted (Frechet-type dendron), and bearing two phosphonate esters on the phenoxy group. These OEG dendrons are structurally close to the dendrons that have been found to improve the dispersibility and stability of iron oxide nanoparticles (IONPs) in aqueous solutions, a critical property for many studies and applications [8,22]. Recent work has established that IONPs grafted with OEG dendrons fitted with fluorinated end-groups form spontaneously adsorbed (Gibbs) films with low interfacial tension, especially when the atmosphere is saturated with a fluorocarbon [23]. As a consequence of this enhanced adsorption, small and stable fluorocarbon-stabilized microbubbles with a shell of phospholipid incorporating IONPs grafted with C_2F_5 -terminated OEG dendrons were obtained [23]. The mixed DMPC/OEG dendron monolayers are indeed model interfaces that can provide insights into the interactions between the components, namely phospholipid and dendron, that form the microbubble shell.

To this end, 10 dendrons were synthesized and investigated that featured two phosphonic esters and three OEG chains, including a longer one, connected by a phenoxyethylcarbamoylphenoxy group. The long OEG chain was fitted with a *t*-Bu, or a hydrocarbon chain (C_6H_{13} or C_8H_{17}), or a partially fluorinated chain ($C_2F_5C_4H_8$ or $C_4F_9C_4H_8$) as the end group (Scheme 1). The number of ethylene glycol groups x was four, six, or eight. First, we have presented the behavior of these dendrons when spread on the surface of water, as studied by compression isotherms, compression/expansion cycles, and Brewster angle microscopy. Second, we have described the monolayer behavior of these OEG dendrons when mixed with a phospholipid, dimyristoylphosphatidylcholine (DMPC).

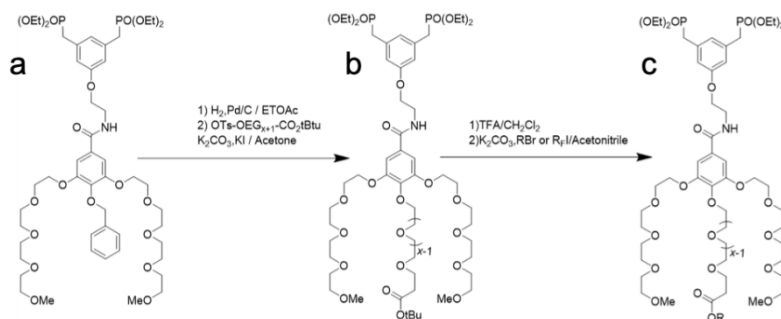


Scheme 1. Molecular structure and schematic representation of the oligo(ethylene glycol) (OEG) dendrons investigated.

2. Results

2.1. Synthesis of OEG Dendrons

The dendrons were obtained via a multistep synthesis (Scheme 2). Starting from the BenzDen dendron precursor [24], the methodology involved the removal of the benzyl group and the introduction of the OEG chain in a basic medium, which provided the $t\text{-BuOEG}_x\text{Den}$ dendrons. After deprotection of the $t\text{-Bu}$ group, the dendrons were alkylated using a hydrocarbon bromide or perfluoroalkyl iodide to give access to the dendrons fitted with a hydrocarbon chain ($C_nH_{2n+1}OEG_8\text{Den}$) or a partially fluorinated chain ($C_nF_{2n+1}C_4H_8OEG_8\text{Den}$).



Scheme 2. Multi-step synthesis of OEG dendrons, starting from (a) the BenzDen precursor, (b) introduction of $t\text{-Bu}$, and (c) alkylation with an alkyl or a perfluoroalkyl halide.

2.2. Langmuir Monolayers of OEG Dendrons Carrying a $t\text{-Bu}$ Group, an Alkyl, or a Partially Fluorinated Chain

2.2.1. Isotherm Characteristics

The surface pressure/molecular area (π/A) isotherms at 25 °C of the 10 OEG dendrons investigated are presented in Figure 1. The isotherms presented the various regimes that can be ascribed to the OEG conformational transitions [7,19,20], by analogy to the behavior observed for diblock copolymers (for example, poly(styrene)-poly(ethylene oxide) [25]. At large molecular areas, liquid-expanded monolayers were observed in which the dendrons were anchored at the interface by the phenyl groups, while the OEG chains lay flat at this interface, forming a so-called “pancake” structure [19,26–28].

Within a homologous series ($t\text{-BuOEG}_x\text{Den}$ or $C_6H_{13}OEG_x\text{Den}$), the extrapolated molecular area A_0 increased with x (Table 1), which confirmed the pancake structure. A break (pseudo-plateau) was observed at a surface pressure π_p . This break was associated with the progressive dissolution of the OEG chains in the water sub-phase [25,26,29]. The extension of the pseudo-plateau did not depend on

x , likely because the increments in x were small. For t -BuOEG $_x$ Den, a significant increase of π_p with x was visible, however (π_p : 6.0–6.5 mN m⁻¹ for $x = 4$ or 6 and 9.6 mN m⁻¹ for $x = 8$), in agreement with earlier reports [30–32]. Although collapse pressures could not be determined, the maximal pressures reached increased with x for t -BuOEG $_x$ Den and C $_n$ H $_{2n+1}$ OEG $_8$ Den ($n = 6$ and 8), reflecting better anchoring at the water surface.

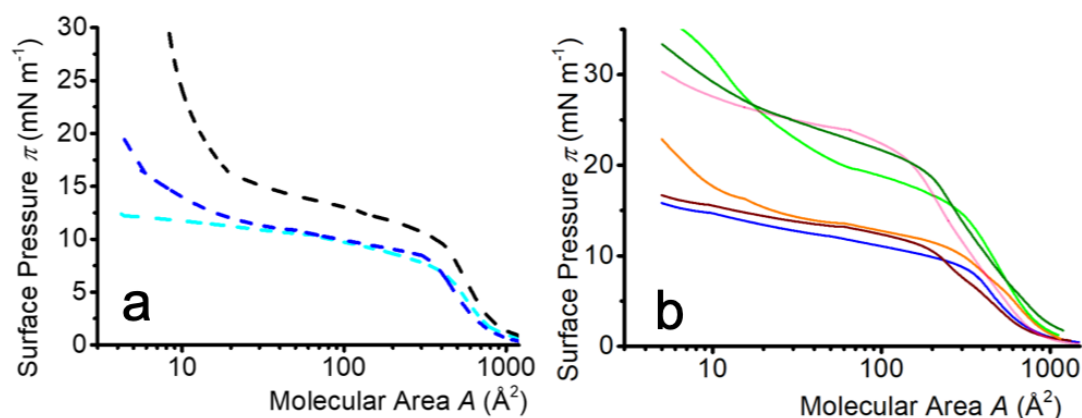


Figure 1. Compression isotherms at 25 °C of Langmuir monolayers of (a) t -BuOEG $_x$ Den ($x = 4$: light blue; $x = 6$: dark blue; $x = 8$: black) and (b) OEG dendrons fitted with hydrophobic chains (C₂F₅C₄H₈OEG₈Den: light green; C₆H₁₃OEG₈Den: orange; C₄F₉C₄H₈OEG₈Den: dark green; C₈H₁₇OEG₈Den: purple; C₆H₁₃OEG₆Den: brown; and C₆H₁₃OEG₄Den: blue).

Table 1. Characteristics of monolayers of OEG dendrons. Extrapolated molecular area in the liquid-expanded phase (A_0) and surface pressure on the plateau (π_p).

Dendrons	A_0 (Å ²) \pm 50 Å ²	π_{plateau} (mN m ⁻¹) \pm 1 mN m ⁻¹
t -BuOEG ₄ Den	750	6.0
t -BuOEG ₆ Den	850	6.5
t -BuOEG ₈ Den	900	9.6
C ₆ H ₁₃ OEG ₄ Den	700	7.2
C ₆ H ₁₃ OEG ₆ Den	720	9.9
C ₆ H ₁₃ OEG ₈ Den	850	9.1
C ₂ F ₅ C ₄ H ₈ OEG ₈ Den	780	13.1
C ₈ H ₁₇ OEG ₈ Den	470	18.3
C ₄ F ₉ C ₄ H ₈ OEG ₈ Den	580	17.7

For a given x value, A_0 was found to be smaller and π_p higher for the dendrons fitted with the most hydrophobic end-groups, such as C₈H₁₇, C₄F₉C₄H₈, or C₂F₅C₄H₈ (Table 1). This suggested that the latter might counteract the anchoring of the OEG chains at the air/water interface by modifying their hydrogen bonds with water, and oppose their dissolution in the water phase. It is also likely that the hydrophobic end-groups promote the coiling of the OEG chain in the *para* position, thus hindering their dissolution in the aqueous sub-phase. It is noteworthy that the increase of π_p was more pronounced for C₂F₅C₄H₈OEG₈Den than for C₆H₁₃OEG₈Den, reflecting the higher hydrophobicity of the fluorinated moieties [33,34]. At low molecular areas (high coverage), only some of the isotherms showed a modest increase in π upon compression, reflecting the fact that a “brush-like” liquid condensed state, in which the OEG chains would be straightened in water, was not reached.

2.2.2. Isotherm Reversibility

In order to investigate whether the dendrons would expand again after compression, two compression–expansion cycles were performed for dendrons fitted with a hydrocarbon chain (C₆H₁₃

or C_8H_{17}) or a partially fluorinated chain ($C_2F_5C_4H_8$ or $C_4F_9C_4H_8$). Hysteresis cycles were recorded both in the liquid-expanded state of the monolayers (Figure 2a) and on the OEG chain conformational transition plateau (Figure 2b). For all dendrons but $C_6H_{13}OEG_8Den$, the isotherms exhibited only minimal hysteresis, reflecting the stability of the monolayers when cycled in the fluid state. The difference in stability between the fluorinated dendron $C_2F_5C_4H_8OEG_8Den$ and its hydrocarbon analog $C_6H_{13}OEG_8Den$ confirmed the stabilizing effect of the C_2F_5 group that contributed to anchoring the monolayer at the interface, owing to the low interfacial tension of the fluorinated chains [35,36]. When the monolayers were successively compressed and expanded on the plateau, the isotherms presented significant hysteresis, which was likely due to the OEG chain conformational transition that induced a desorption of the dendrons from the interface.

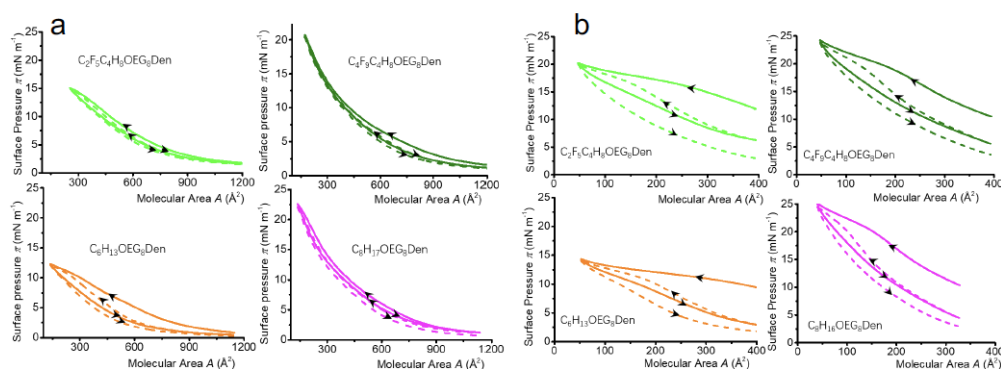


Figure 2. Compression–expansion cycles of Langmuir monolayers of OEG dendrons fitted with hydrophobic end-groups, recorded in (a) the liquid-expanded regime and (b) the plateau. The first and second compression–decompression cycles are indicated by solid and dashed lines, respectively.

2.2.3. Brewster Angle Microscopy and Atomic Force Microscopy

The monolayers of OEG dendrons fitted with a hydrocarbon chain (C_6H_{13} or C_8H_{17}) or a partially fluorinated chain ($C_2F_5C_4H_8$ or $C_4F_9C_4H_8$) were investigated by BAM and AFM (Figure 3). BAM images indicated that the hydrocarbon dendrons $C_6H_{13}OEG_8Den$ and $C_8H_{17}OEG_8Den$ formed fluid monolayers at all surface pressures. By contrast, the two fluorinated dendrons ($C_2F_5C_4H_8OEG_8Den$ and $C_4F_9C_4H_8OEG_8Den$) formed crystalline-like domains from the beginning of the compression. These domains persisted throughout compression. A variation of the domain size was also observed, probably reflecting some coalescence.

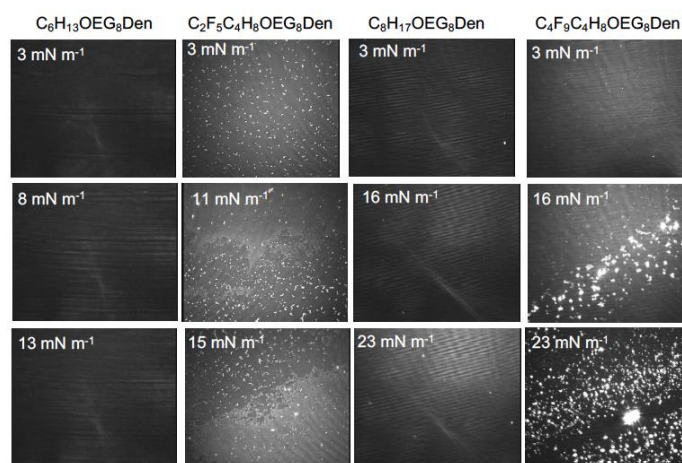


Figure 3. Brewster angle microscopy (BAM) images of the monolayers of OEG dendrons fitted with hydrogenated or fluorinated end-groups. Size of the images is $600 \times 500 \mu m^2$.

2.3. Mixed Langmuir Monolayers of Phospholipid and OEG Dendrons

2.3.1. Characteristics of the Compression Isotherms

Compression isotherms and BAM images were recorded for mixed monolayers of DMPC and OEG dendrons carrying hydrocarbon chains ($C_6H_{13}OEG_8Den$ and $C_8H_{17}OEG_8Den$), or partially fluorinated chains ($C_2F_5C_4H_8OEG_8Den$ and $C_4F_9C_4H_8OEG_8Den$). A DMPC/OEG dendron molar ratio of 75:25 was set, this composition having been selected as optimal for the formulation of microbubbles [23]. Most commercially available microbubble-based contrast agents indeed possess a shell made of phospholipids [37–39]. The compression isotherms of DMPC and of the mixed monolayers are displayed in Figure 4. The DMPC monolayer presented a monotonous π/A curve, typical of a liquid-expanded state, throughout compression. The isotherms of the mixed monolayers presented a significant shift to larger molecular area and a pseudo-plateau, indicating that both components were present at the interface. The π_p values on the plateaus corresponded well to the π_p values observed for dendrons as the sole monolayer component. At small molecular areas, the isotherms of the mixtures coincided with those of the DMPC monolayer, indicating that dendrons were likely expelled from the phospholipid monolayer.

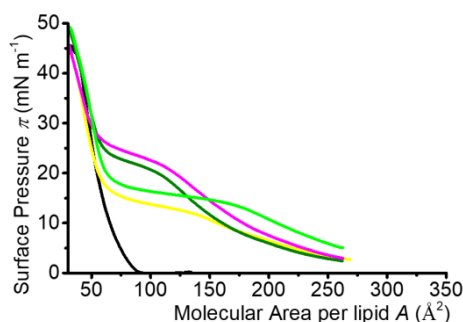


Figure 4. Compression isotherms of dimyristoylphosphatidylcholine (DMPC) (black) and DMPC/OEG dendron mixed Langmuir monolayers (DMPC/dendron molar ratio: 75:25; $C_2F_5C_4H_8OEG_8Den$: green; $C_6H_{13}OEG_8Den$: orange; $C_4F_9C_4H_8OEG_8Den$: dark green; $C_8H_{16}OEG_8Den$: purple). Temperature was 25 °C.

Next, the miscibility of DMPC and the dendrons in mixed monolayers was examined by plotting the variation of the molecular area A_0 versus the dendron molar ratio (Figure 5). Positive deviations from ideality were determined using the additivity rule [40,41]. For dendrons fitted with the longest chains, the deviations were observed to affect monolayers with a larger dendron molar ratio. Partial fluorination of the hydrophobic chain also increased the deviation to ideality. This indicated limited miscibility with repulsive interactions between the monolayer components.

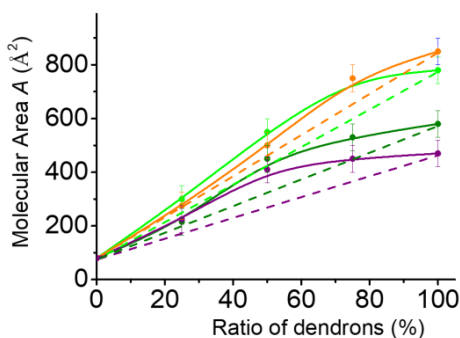


Figure 5. Variation of the extrapolated molecular area A_0 as a function of molar ratio of dendrons in DMPC monolayers. $C_6H_{13}OEG_8Den$ (orange); $C_2F_5C_4H_8OEG_8Den$ (light green); $C_8H_{17}OEG_8Den$ (purple); and $C_4F_9C_4H_8OEG_8Den$ (dark green).

2.3.2. Isotherm Reversibility

Mixed DMPC/OEG dendron monolayers were subjected to compression–expansion cycles in the transition regime (Figure 6). Strong hysteresis was observed during decompression for both fluorinated and hydrocarbon dendrons, which indicated that the monolayer components did not re-spread easily at the interface due to intermolecular interactions, suggesting the possible formation of crystalline-like domains. During the second compression π strongly decreased, which indicated that the dendrons were progressively expelled from the monolayers when the mixed monolayers were compressed at $\pi > \pi_p$.

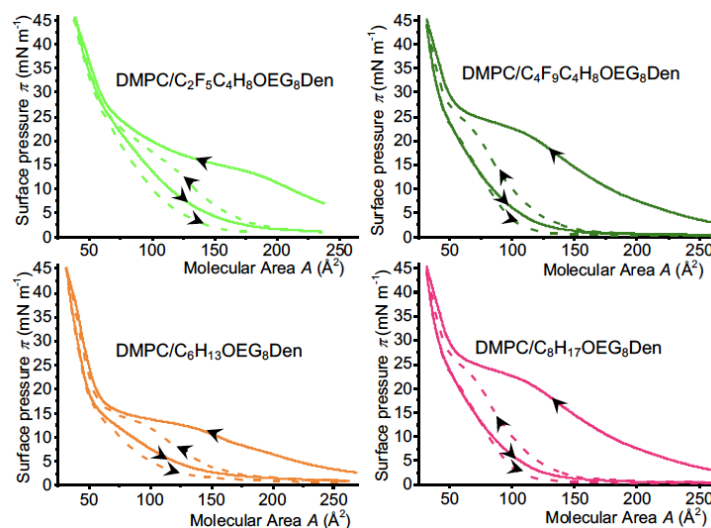


Figure 6. Hysteresis compression–expansion cycles of mixed DMPC/OEG dendrons Langmuir monolayers at the air/water interface (DMPC/dendron molar ratio: 75:25). First and second compression–expansion cycles are indicated by solid and dashed lines, respectively.

2.3.3. Brewster Angle Microscopy and Atomic Force Microscopy

Representative BAM images of the mixed DMPC/OEG dendron monolayers are displayed in Figure 7. The DMPC monolayer was in a liquid-expanded state throughout compression, which resulted in a featureless BAM image.

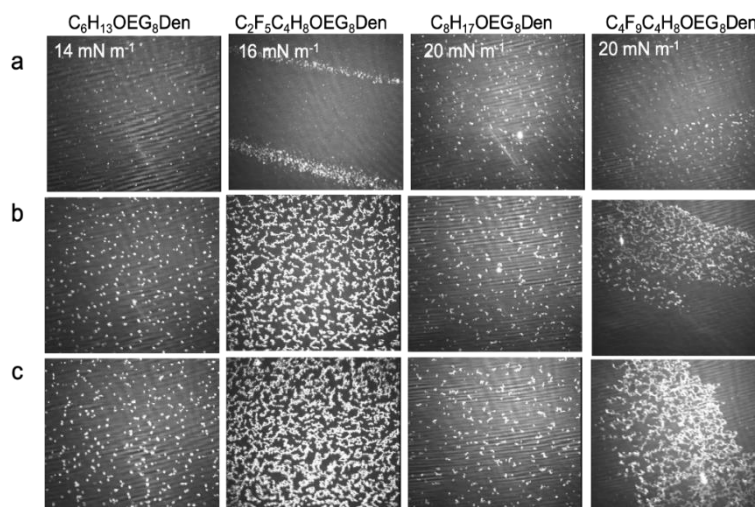


Figure 7. BAM images of DMPC/OEG dendron mixed Langmuir monolayers at the air/water interface (a) at the transition, (b) at 30 mN m^{-1} , and (c) after collapse at 40 mN m^{-1} .

By contrast, the images of the mixed monolayers displayed domains (white features) for all dendrons and all surface pressures. These domains became more numerous as π increased. It is noteworthy that even the dendrons fitted with the hydrocarbon chains, which formed fluid monolayers when spread alone on the surface of water, formed domains when mixed with DMPC. The domains were particularly numerous in the case of $C_2F_5C_4H_8OEG_8Den$, owing to the increased lipophobicity of the fluorinated chains.

Atomic force microscopy was performed in order to get more information on the domains formed in the DMPC/ $C_2F_5C_4H_8OEG_8Den$ (75:25 molar ratio) mixed monolayers. The micrographs showed that, when the monolayers were transferred on the plateau (14 mN m^{-1}), small circular domains were predominantly formed, along with some rare coiled aggregates (Figure 8a). When π increased, the number of coiled aggregates and their size increased (Figure 8b). At 44 mN m^{-1} , that is, near collapse, a dendritic pattern of dendrons was formed that quasi-totally covered the DMPC monolayer (Figure 8c). This indicated that the dendrons were progressively expelled from the phospholipid monolayer. The mean height of the aggregates above the DMPC monolayer was consistent with a bilayer of dendrons ($\sim 6 \text{ nm}$). Furthermore, it was observed that the height of the aggregates increased slightly, but significantly, with the surface pressure at which the monolayers were transferred. For example, the measured heights were 5.1, 6.3, and $7.0 \pm 0.3 \text{ nm}$ for transfer pressures of 14, 30, and 44 mN m^{-1} , respectively (Figure 8c). This trend also supported the view that the dendron aggregates, which were initially embedded in the DMPC monolayer, were progressively expelled, self-assembled into strands, and eventually formed plaques that covered the monolayer.

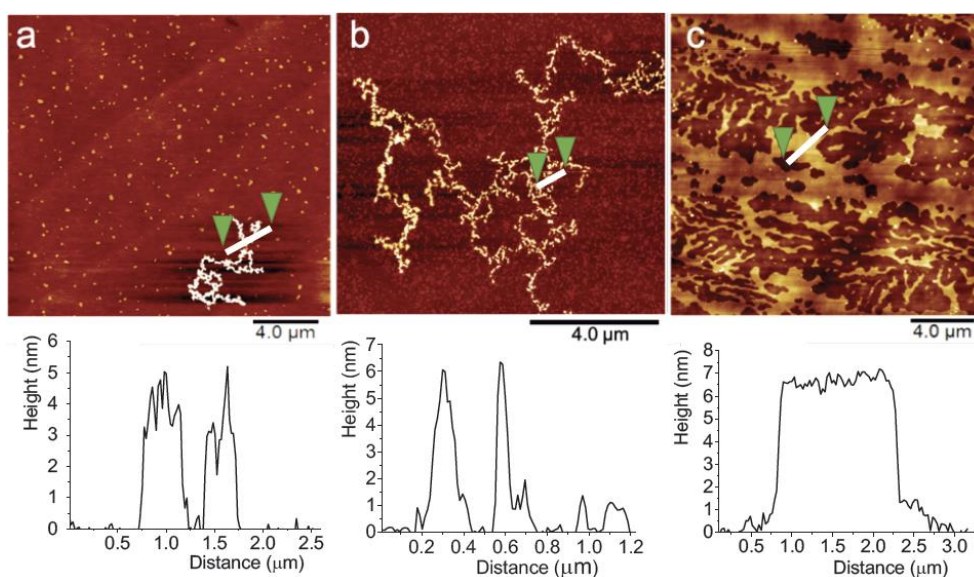


Figure 8. Atomic force microscopy (AFM) images and height profiles of mixed DMPC/ $C_2F_5C_4H_8OEG_8Den$ monolayers (molar ratio: 75:25) after transfer onto silicon wafers at (a) 14 mN m^{-1} , (b) 30 mN m^{-1} , and (c) 44 mN m^{-1} .

3. Conclusions and Perspectives

Our main objective was to investigate the interfacial behavior of phospholipid-embedded OEG dendrons containing a *t*-Bu, a hydrocarbon, or a fluorinated end-group. These compounds are structurally close to the dendrons used to coat iron oxide nanoparticles developed for imaging and hyperthermia procedures. These dendronized magnetic nanoparticles are presently being investigated in combination with phospholipids to stabilize medical microbubbles. All the experiments conducted in this study indicated that OEG dendrons were expelled during compression, both from the air/water interface when they were spread as the sole component, and from DMPC monolayers, when they were co-spread at the interface with this phospholipid. When the surface density of dendrons triggered the

OEG conformational transition, the dendrons were desorbed from the interface and expelled in the aqueous phase. This means that the three OEG chains of unequal lengths were not hydrophilic enough to enable the formation of a brush-like liquid condensed phase, as has been observed with PEG- and some OEGylated dendrons. These mixed phospholipid/dendron monolayers can be viewed as model interfaces of the monolayers that form the shells of medical microbubbles. In this regard, this work suggests that the propensity of OEG dendrons to be squeezed out from phospholipid monolayers could be exploited to facilitate the delivery of dendronized magnetic nanoparticles *in vivo*, and most particularly for the combined use of ultrasound and magnetic resonance tumor imaging modalities.

4. Materials and Methods

4.1. Materials

1,2-dimyristoylphosphatidylcholine (DMPC) was purchased as a dry powder (99% purity) from Avanti Polar Lipids (Alabaster, AL, USA) and used as received. Water was purified using a Millipore system (surface tension 72.1 mN m^{-1} at $20 \text{ }^\circ\text{C}$, resistivity: $18.2 \text{ M}\Omega \text{ cm}$).

4.2. Synthesis of the Dendrons

***t*-BuOEG x Den** ($x = 4, 6, 8$): Pd/C 10% (0.1 equiv.) was added to a solution of BenzDen (1.0 equiv.) in EtOAc (0.1 M). The heterogeneous solution was backfilled five times with an atmosphere of hydrogen, then vigorously stirred at room temperature overnight. The catalyst was filtered over Celite and the crude product was concentrated under reduced pressure and dissolved in acetone (0.1 M), after which K_2CO_3 (1.5 equiv.) and OTsOEG x CO $_2$ *t*-Bu (1.1 equiv.) were added. The resulting heterogenous solution was stirred at reflux for 16 h and cooled to room temperature. After filtration, the crude product was concentrated under reduced pressure. Chromatography on silica gel afforded the final product as a yellow oil.

***t*-Bu-OEG $_4$ Den:** ^1H NMR (500 MHz, CDCl_3): δ (ppm): 7.11 (s, 2H), 6.88 (brs, 1H), 6.82 (s, 1H), 6.78 (d, $J = 2.2 \text{ Hz}$, 1H), 4.22 (t, $J = 4.7 \text{ Hz}$, 4H), 4.14 (t, $J = 4.9 \text{ Hz}$, 2H), 4.02 (qt, $J = 7.4 \text{ Hz}$, 8H), 3.85 (t, $J = 5.1 \text{ Hz}$, 4H), 3.82–3.77 (m, 4H), 3.72–3.60 (m, 56H), 3.54–3.52 (m, 4H), 3.36 (s, 6H), 3.09 (d, $^2J_{\text{P-H}} = 22.3 \text{ Hz}$, 4H), 2.50 (t, $J = 6.2 \text{ Hz}$, 2H), 1.44 (s, 9H), 1.25 (t, $J = 7.2 \text{ Hz}$, 12H). ^{13}C NMR (125 MHz, CDCl_3): δ (ppm): 170.9, 167.2, 152.4, 133.3, 129.5, 114.6, 107.3, 80.5, 72.3, 71.9, 70.6–70.5 (several peaks), 70.3, 69.7, 69.1, 66.9, 66.7, 62.1 (d, $^2J_{\text{C-P}} = 6.6 \text{ Hz}$), 59.0, 39.5, 36.2, 33.6 (d, $^1J_{\text{C-P}} = 138.4 \text{ Hz}$), 28.1, 16.4 (d, $^3J_{\text{C-P}} = 5.4 \text{ Hz}$). ^{31}P NMR (202 MHz, CDCl_3): δ (ppm): 26.0.

***t*-Bu-OEG $_6$ Den:** ^1H NMR (500 MHz, CDCl_3): δ (ppm): 7.11 (s, 2H), 6.88 (brs, 1H), 6.82 (s, 1H), 6.78 (d, $J = 2.2 \text{ Hz}$, 1H), 4.22 (t, $J = 4.7 \text{ Hz}$, 4H), 4.14 (t, $J = 4.9 \text{ Hz}$, 2H), 4.02 (qt, $J = 7.4 \text{ Hz}$, 8H), 3.85 (t, $J = 5.1 \text{ Hz}$, 4H), 3.82–3.77 (m, 4H), 3.72–3.60 (m, 56H), 3.54–3.52 (m, 4H), 3.36 (s, 6H), 3.09 (d, $^2J_{\text{P-H}} = 22.3 \text{ Hz}$, 4H), 2.50 (t, $J = 6.2 \text{ Hz}$, 2H), 1.44 (s, 9H), 1.25 (t, $J = 7.2 \text{ Hz}$, 12H). ^{13}C NMR (125 MHz, CDCl_3): δ (ppm): 170.9, 167.2, 158.8, 152.5, 141.7, 133.3, 129.5, 124.4, 114.6, 107.3, 80.5, 72.3, 71.9, 70.7–70.3 (several peaks), 69.7, 69.1, 66.9, 66.7, 62.1 (d, $^2J_{\text{C-P}} = 7.2 \text{ Hz}$), 59.0, 39.5, 36.2, 33.6 (d, $^1J_{\text{C-P}} = 137.8 \text{ Hz}$), 28.1, 16.4 (d, $^3J_{\text{C-P}} = 5.6 \text{ Hz}$). ^{31}P NMR (202 MHz, CDCl_3): δ (ppm): 26.0.

***t*-Bu-OEG $_6$ Den:** See characteristics in [24].

$\text{C}_n\text{H}_{2n+1}\text{OEG}_8\text{Den}$ ($n = 6$ and 8) and $\text{C}_n\text{F}_{2n+1}\text{C}_4\text{H}_8\text{OEG}_8\text{Den}$ ($n = 2$ and 4): TFA (5.0 equiv.) was added to a solution of *t*-BuOEG $_8$ Den (1.0 equiv.) in CH_2Cl_2 (0.1 M). The solution was stirred at room temperature for 4 h, concentrated under reduced pressure, dissolved in acetonitrile (0.1 M) before K_2CO_3 (2.0 equiv.) and the appropriate alkyl (or *F*-alkyl) halide (4.0 equiv., $\text{C}_6\text{H}_{13}\text{Br}$, $\text{C}_8\text{H}_{17}\text{Br}$, $\text{C}_2\text{F}_5\text{C}_4\text{H}_8\text{I}$, or $\text{C}_4\text{F}_9\text{C}_4\text{H}_8\text{I}$) was added. After stirring at reflux for 16 h and cooling to room temperature, the solid was filtered and the crude product was concentrated under reduced pressure. Chromatography on silica gel afforded the product as a yellow oil.

C₆H₁₃OEG₈Den: ¹H NMR (500 MHz, CDCl₃): δ (ppm): 7.10 (s, 2H), 6.77 (s, 1H), 6.76 (s, 2H), 4.21 (t, *J* = 4.9 Hz, 4H), 4.18 (t, *J* = 5.1 Hz, 2H), 4.13 (t, *J* = 5.1 Hz, 2H), 4.07 (t, *J* = 6.8 Hz, 2H), 4.04–3.97 (m, 10H), 3.84 (t, *J* = 4.9 Hz, 4H), 3.81–3.76 (m, 6H), 3.73 (t, *J* = 6.4 Hz, 2H), 3.71–3.58 (m, 50H), 3.53–3.51 (m, 4H), 3.35 (s, 6H), 3.08 (d, ²*J*_{P-H} = 21.6 Hz, 4H), 2.58 (t, *J* = 6.5 Hz, 2H), 1.61 (qt, *J* = 9.5 Hz, 2H), 1.38–1.26 (m, 8H), 1.24 (t, *J* = 7.1 Hz, 12H), 0.88 (t, *J* = 7.1 Hz, 3H). ¹³C NMR (125 MHz, CDCl₃): δ (ppm): 171.6, 167.3, 158.6, 152.4, 141.4, 133.3, 129.6, 124.0, 114.7, 107.3, 72.3, 71.9, 70.7–70.4 (several peaks), 69.7, 69.0, 66.7, 64.7, 62.3, 59.0, 39.6, 35.1, 34.1, 33.0, 31.4, 28.5, 25.5, 22.5, 16.4, 14.0. ³¹P NMR (202 MHz, CDCl₃): δ (ppm): 26.0.

C₈H₁₇OEG₈Den: ¹H NMR (500 MHz, CDCl₃): δ (ppm): 7.10 (s, 2H), 6.88 (brs, 1H), 6.80 (s, 1H), 6.76 (s, 2H), 4.21 (t, *J* = 5.2 Hz, 4H), 4.18 (t, *J* = 5.2 Hz, 2H), 4.13 (t, *J* = 5.2 Hz, 2H), 4.06 (t, *J* = 6.8 Hz, 2H), 4.04–3.97 (m, 8H), 3.84 (t, *J* = 4.9 Hz, 4H), 3.80–3.77 (m, 4H), 3.74 (t, *J* = 6.7 Hz, 2H), 3.70–3.59 (m, 50H), 3.53–3.51 (m, 4H), 3.35 (s, 6H), 3.07 (d, ²*J*_{P-H} = 21.6 Hz, 4H), 2.58 (t, *J* = 6.7 Hz, 2H), 1.60 (qt, *J* = 9.5 Hz, 2H), 1.36–1.23 (m, 34H), 0.87 (t, *J* = 6.9 Hz, 3H). ¹³C NMR (125 MHz, CDCl₃): δ (ppm): 171.6, 167.3, 158.8, 152.5, 141.7, 133.2, 129.5, 124.1, 114.7, 107.4, 72.4, 71.9, 70.7–70.4 (several peaks), 69.7, 69.1, 66.7, 64.7, 62.2, 59.0, 39.6, 35.1, 34.2, 33.1, 31.9, 29.6, 29.5, 29.3, 29.2, 26.3, 25.9, 22.7, 16.4, 14.1. ³¹P NMR (202 MHz, CDCl₃): δ (ppm): 26.0 ppm.

C₂F₅C₄H₈OEG₈Den: ¹H NMR (500 MHz, CDCl₃): δ (ppm): 7.10 (s, 2H), 7.00 (brs, 1H), 6.80 (s, 1H), 6.76 (s, 2H), 4.20 (t, *J* = 4.4 Hz, 4H), 4.17 (t, *J* = 4.6 Hz, 2H), 4.13–4.09 (m, 4H), 4.00 (qt, *J* = 7.4 Hz, 8H), 3.83 (t, *J* = 4.7 Hz, 4H), 3.79–3.75 (m, 4H), 3.73 (t, *J* = 6.4 Hz, 2H), 3.70–3.60 (m, 50H), 3.52–3.50 (m, 4H), 3.34 (s, 6H), 3.07 (d, ²*J*_{P-H} = 22.2 Hz, 4H), 2.58 (t, *J* = 6.6 Hz, 2H), 2.11–1.99 (m, 4H), 1.74–1.62 (m, 4H), 1.23 (t, *J* = 7.1 Hz, 12H). ¹³C NMR (125 MHz, CDCl₃): δ (ppm): 171.5, 167.2, 158.6, 152.4, 141.4, 133.2, 129.5, 124.0, 114.7, 107.3, 72.3, 71.9, 70.6–70.4 (several peaks), 69.7, 69.0, 66.7, 66.5, 63.6, 62.2 (d, ²*J*_{C-P} = 6.9 Hz), 59.0, 39.5, 35.0, 34.1, 33.0, 30.9, 30.4, 30.2, 30.0, 29.7, 28.0, 17.1, 16.4 (d, ³*J*_{C-P} = 5.8 Hz). ³¹P NMR (202 MHz, CDCl₃): δ (ppm): 26.3. ¹⁹F NMR (282 MHz, CDCl₃): δ (ppm): –85.4, –118.3.

C₄F₉C₄H₈OEG₈Den: ¹H NMR (500 MHz, CDCl₃): δ (ppm): 7.09 (s, 2H), 6.88 (brs, 1H), 6.79 (s, 1H), 6.75 (s, 2H), 4.20 (t, *J* = 4.9 Hz, 4H), 4.17 (t, *J* = 4.9 Hz, 2H), 4.11–4.09 (m, 4H), 4.03–3.96 (m, 8H), 3.82 (t, *J* = 5.1 Hz, 4H), 3.79–3.75 (m, 4H), 3.73 (t, *J* = 6.5 Hz, 2H), 3.69–3.56 (m, 48H), 3.51–3.50 (m, 4H), 3.33 (s, 6H), 3.07 (d, ²*J*_{P-H} = 21.6 Hz, 4H), 2.57 (t, *J* = 6.6 Hz, 2H), 2.18–2.02 (m, 4H), 1.74–1.63 (m, 4H), 1.23 (t, *J* = 7.0 Hz, 12H). ¹³C NMR (125 MHz, CDCl₃): δ (ppm): 171.5, 167.2, 158.6, 152.4, 141.5, 133.3, 129.5, 124.0, 114.6, 107.3, 72.2, 71.9, 70.7–70.4 (several peaks), 69.7, 69.1, 66.7, 63.6, 62.2, 59.0, 39.5, 35.0, 34.2, 33.1, 30.4, 28.0, 17.0, 16.4. ³¹P NMR (202 MHz, CDCl₃): δ (ppm): 26.0 ppm. ¹⁹F NMR (480 MHz, CDCl₃): δ (ppm): –126.0, 124.5, –114.5, –81.0.

4.3. Langmuir Monolayers

The surface pressure (π) versus molecular area (*A*) isotherms were recorded using a Langmuir minitrough (KSV NIMA, Finland) equipped with two movable barriers (initial area: 365 × 75 mm², compression speed: 10 cm² min^{−1}, which corresponded to a reduction of the total area of ~3.6% min^{−1}). π was measured using the Wilhelmy plate (paper) method. The trough was maintained at 25 ± 0.5 °C. Solutions of OEG dendrons (1 mmol L^{−1}) in chloroform were spread on the surface of water (320 mL). Subsequently, 15 min was allowed for chloroform to evaporate and the film to equilibrate before compression was initiated. All the experiments were performed at least three times. Since our Langmuir trough only allowed for a surface area compression of about 10, isotherms were recorded in three separate experiments.

4.4. Atomic Force Microscopy (AFM)

The monolayers of dendrons or DMPC/dendron mixtures were compressed up to the desired surface pressure and transferred at constant surface pressure onto silicon wafers using the Langmuir–Blodgett technique (one monolayer transferred; lift speed: 1 mm min^{−1}). Silicon wafers were cleaned for 30 min in a sonication bath containing ethanol/milliQ water (1:1 vol:vol), followed

by 2 min in a plasma cleaner. The LB films were immediately analyzed by AFM after preparation. Images of the transferred films were recorded in tapping mode (AFM multimode 8, Bruker, Santa Barbara, CA, USA). The cantilever (Budget Sensors) had a 3–10 nm radius silicon tip. The typical resonance frequency was 300 kHz and the spring constant was 40 N m⁻¹. At least three different samples were analyzed and several areas were scanned on the silicon wafer for each sample. Errors of the measurements along the z axis were estimated to be ± 0.5 nm.

4.5. Brewster Angle Microscopy (BAM)

When a laser beam polarized parallel to the plane of incidence hits the air/water interface at an angle of 53.15°, which is called the Brewster angle ($= \arctan n_{\text{water}}/n_{\text{air}}$, with n the refractive index), there is essentially no light reflected. However, the presence of a monolayer at the interface alters the Brewster conditions, which results in some light being reflected. The intensity of the reflected light is a function of film thickness and refractive index. With an optical microscope set at the Brewster angle, the water surface appears dark and the thin film brighter. In this way, BAM allows the direct observation of some morphological characteristics of monolayers. A Bam2Plus microscope (NFT, Gottingen, Germany) equipped with a KSV Minitrough Langmuir system (320 × 75 mm²) was used for the experiments. The volumes of dendron solution (1 mM) and DMPC/dendron mixtures (molar ratio: 75:25) deposited on the surface were 5 µL and 20 µL, respectively. Snapshots were captured when the monolayers were compressed up to desired pressures at a compression speed of 1.5 cm² min⁻¹. The scale of the images is 600 × 500 µm.

Author Contributions: D.S. performed the experimental work. D.-V.N. and D.F.-F. contributed to the design and synthesized the dendrons. M.M. and J.-L.G. participated to the methodology and design of AFM and BAM experiments. M.P.K. conceived and supervised the project, and wrote the article. All authors commented the results and edited the article.

Funding: The European Regional Development Fund (ERDF) in the framework of the INTERREG V Upper Rhine program.

Acknowledgments: The authors acknowledge the European Regional Development Fund (ERDF) in the framework of the INTERREG V Upper Rhine program “Transcending borders with every project” for financing the NANOTRANSMED project, including Ph.D. (D.S.) and post-doc (D.-V.N.) scholarships.

Conflicts of Interest: The authors declare no conflict of interest.

References

1. Bosman, A.W.; Janssen, H.M.; Meijer, E.W. About dendrimers: Structure, physical properties, and applications. *Chem. Rev.* **1999**, *99*, 1665–1688. [[CrossRef](#)]
2. Grayson, S.M.; Frechet, J.M.J. Convergent dendrons and dendrimers: From synthesis to applications. *Chem. Rev.* **2001**, *101*, 3819–3867. [[CrossRef](#)]
3. Kannan, R.M.; Nance, E.; Kannan, S.; Tomalia, D.A. Emerging concepts in dendrimer-based nanomedicine: From design principles to clinical applications. *J. Int. Med.* **2014**, *276*, 579–617. [[CrossRef](#)]
4. Rosen, B.M.; Wilson, D.A.; Wilson, C.J.; Peterca, M.; Won, B.C.; Huang, C.H.; Lipski, L.R.; Zeng, X.B.; Ungar, G.; Heiney, P.A.; et al. Predicting the structure of supramolecular dendrimers via the analysis of libraries of AB₃ and constitutional isomeric AB₂ biphenylpropyl ether self-assembling dendrons. *J. Am. Chem. Soc.* **2009**, *131*, 17500–17521. [[CrossRef](#)]
5. Leshchiner, I.; Boiko, N.; Kumar, J.; Richardson, R.M.; Muzafarov, A.; Shibaev, V. Synthesis and physical behavior of amphiphilic dendrimers with layered organization of hydrophilic and hydrophobic blocks. *Colloid Polym. Sci.* **2012**, *291*, 927–936. [[CrossRef](#)]
6. Kumar, A.; Tyagi, S.; Singh, R.; Tyagi, Y.K. Synthesis, characterisation and self-assembly studies of dendron-based novel non-ionic amphiphiles. *New J. Chem.* **2019**, *43*, 1025–1031. [[CrossRef](#)]
7. Kampf, J.P.; Frank, C.W.; Malmstrom, E.E.; Hawker, C.J. Stability and molecular conformation of poly(benzyl ether) monodendrons with oligo(ethylene glycol) tails at the air-water interface. *Langmuir* **1999**, *15*, 227–233. [[CrossRef](#)]

8. Basly, B.; Felder-Flesch, D.; Perriat, P.; Billotey, C.; Taleb, J.; Pourroy, G.; Begin-Colin, S. Dendronized iron oxide nanoparticles as contrast agents for MRI. *Chem. Commun.* **2010**, *46*, 985–987. [[CrossRef](#)] [[PubMed](#)]
9. Walter, A.; Garofalo, A.; Parat, A.; Taleb, J.; Bonazza, P.; Jouhannaud, J.; Pourroy, G.; Voirin, E.; Billotey, C.; Laurent, S.; et al. Validation of a dendron concept to tune colloidal stability, MRI relaxivity and bioelimination of functional nanoparticles. *J. Mater. Chem. B* **2015**, *3*, 1484–1494. [[CrossRef](#)]
10. Pasut, G.; Paolino, D.; Celia, C.; Mero, A.; Joseph, A.S.; Wolfram, J.; Cosco, D.; Schiavon, O.; Shen, H.; Fresta, M. Polyethylene glycol (PEG)-dendron phospholipids as innovative constructs for the preparation of super stealth liposomes for anticancer therapy. *J. Control. Release* **2015**, *199*, 106–113. [[CrossRef](#)] [[PubMed](#)]
11. Kang, S.Z.; Xu, S.L.; Deng, G.J.; Wu, P.; Fan, Q.H.; Wang, C.; Wan, L.J.; Bai, C.L. Langmuir film behaviors of dendrons at water-air interface. *Chem. Phys. Lett.* **2003**, *370*, 542–547. [[CrossRef](#)]
12. Giner, I.; Haro, M.; Gascon, I.; del Barrio, J.; Lopez, M.C. Air-water interfacial behavior of linear-dendritic block copolymers containing PEG and azobenzene chromophores. *J. Colloid Interface Sci.* **2011**, *359*, 389–398. [[CrossRef](#)] [[PubMed](#)]
13. Ahmad, F.; Shin, K. Dendrimers at the air-water interface: Surface dynamics and molecular ordering. *Int. J. Nanotechnol.* **2006**, *3*, 353–371. [[CrossRef](#)]
14. Park, J.Y.; Advincula, R.C. Nanostructuring polymers, colloids, and nanomaterials at the air–water interface through Langmuir and Langmuir–Blodgett techniques. *Soft Matter* **2011**, *7*, 9829. [[CrossRef](#)]
15. Genson, K.L.; Vaknin, D.; Villacencio, O.; McGrath, D.V.; Tsukruk, V.V. Microstructure of amphiphilic monodendrons at the air-water interface. *J. Phys. Chem. B* **2002**, *106*, 11277–11284. [[CrossRef](#)]
16. Redon, R.; Carreon-Castro, M.P.; Mendoza-Martinez, F.J. Langmuir-blodgett films of supported polyester dendrimers. *ISRN Org. Chem.* **2012**, 906839. [[CrossRef](#)]
17. Su, A.H.; Tan, S.S.; Thapa, P.; Flanders, B.N.; Ford, W.T. Highly ordered Langmuir-Blodgett films of amphiphilic poly(propylene imine) dendrimers. *J. Phys. Chem. C* **2007**, *111*, 4695–4701. [[CrossRef](#)]
18. Qin, L.; Duan, P.-F.; Liu, M.-H. Interfacial assembly and host–guest interaction of anthracene-conjugated l-glutamate dendron with cyclodextrin at the air/water interface. *Chin. Chem. Lett.* **2014**, *25*, 487–490. [[CrossRef](#)]
19. Felipe, M.J.; Llore, N.E.; Pernites, R.B.; Nguyen, T.; Ponnampati, R.; Advincula, R.C. Interfacial behavior of OEG-linear dendron monolayers: Aggregation, nanostructuring, and electropolymerizability. *Langmuir* **2011**, *27*, 9327–9336. [[CrossRef](#)]
20. Degen, P.; Wyszogrodzka, M.; Strotges, C. Film formation of nonionic dendritic amphiphiles at the water surface. *Langmuir* **2012**, *28*, 12438–12442. [[CrossRef](#)]
21. Degen, P.; Wieland, D.C.; Strotges, C. Mixed layers of nonionic dendritic amphiphiles and DPPC at the water surface. *Langmuir* **2015**, *31*, 11851–11857. [[CrossRef](#)]
22. Felder-Flesch, D. *Dendrimers in Nanomedicine*; Pan Stanford Publishing Pte. Ltd.: Singapore, 2016.
23. Shi, D.; Wallyn, J.; Nguyen, D.-V.; Perton, F.; Felder-Flesch, D.; Bégin-Colin, S.; Maaloum, M.; Krafft, M.P. Microbubbles decorated with dendronized magnetic nanoparticles for biomedical imaging. Effective stabilization via fluororous interactions. *Beilstein J. Nanotechnol.* **2019**, *10*, 2103–2115. [[CrossRef](#)]
24. Garofalo, A.; Parat, A.; Bordeianu, C.; Ghobril, C.; Kueny-Stotz, M.; Walter, A.; Jouhannaud, J.; Begin-Colin, S.; Felder-Flesch, D. Efficient synthesis of small-sized phosphonated dendrons: Potential organic coatings of iron oxide nanoparticles. *New J. Chem.* **2014**, *38*, 5226–5239. [[CrossRef](#)]
25. Silva, A.M.G.d.; Filipe, E.J.M.; d'Oliveira, J.M.R.; Martinho, J.M.G. Interfacial behavior of poly(styrene)-poly(ethylene oxide) diblock copolymer monolayers at the air-water interface. Hydrophilic block chain length and temperature influence. *Langmuir* **1996**, *12*, 6547–6553. [[CrossRef](#)]
26. Matmour, R.; Joncheray, T.J.; Gnanou, Y.; Duran, R.S. Two-dimensional polymeric nanomaterials through cross-linking of polybutadiene-b-poly(ethylene oxide) monolayers at the air/water interface. *Langmuir* **2007**, *23*, 649–658. [[CrossRef](#)] [[PubMed](#)]
27. Prasitnok, K.; Wilson, M.R. A coarse-grained model for polyethylene glycol in bulk water and at a water/air interface. *Phys. Chem. Chem. Phys.* **2013**, *15*, 17093–17104. [[CrossRef](#)]
28. Schöne, A.-C.; Roch, T.; Schulz, B.; Lendlein, A. Evaluating polymeric biomaterial-environment interfaces by Langmuir monolayer techniques. *Interface* **2017**, *14*, 20161028. [[CrossRef](#)]
29. Kuzmenka, D.J.; Granick, S. Collapse of poly(ethylene oxide) monolayers. *Macromolecules* **1988**, *21*, 779–782. [[CrossRef](#)]

30. Bijsterbosch, H.D.; de Haan, V.O.; de Graaf, A.W.; Mellema, M.; Leermakers, F.A.M.; Cohen Stuart, M.A.; van Well, A.A. Tethered adsorbing chains: Neutron reflectivity and surface pressure of spread diblock copolymer monolayers. *Langmuir* **1995**, *11*, 4467–4473. [[CrossRef](#)]
31. Fauré, M.C.; Bassereau, P.; Carignano, M.A.; Szleifer, I.; Gallot, Y.; Andelman, D. Monolayers of diblock copolymer at the air-water interface: The attractive monomer-surface case. *Eur. Phys. J. B* **1998**, *3*, 365–375.
32. Deschênes, L.; Saint-Germain, F.; Lyklema, J. Langmuir monolayers of non-ionic polymers: Equilibrium or metastability? Case study of PEO and its PPO-PEO diblock copolymers. *J. Colloid Interface Sci.* **2015**, *449*, 494–505.
33. Krafft, M.P.; Riess, J.G. Chemistry, physical chemistry and uses of molecular fluorocarbon-hydrocarbon diblocks, triblocks and related compounds—Unique apolar components for self-assembled colloid and interface engineering. *Chem. Rev.* **2009**, *109*, 1714–1792. [[CrossRef](#)]
34. Krafft, M.P. Large organized surface domains self-assembled from non-polar amphiphiles. *Acc. Chem. Res.* **2012**, *45*, 514–524. [[CrossRef](#)] [[PubMed](#)]
35. Smart, B.E. Characteristics of C-F systems. In *Organofluorine Chemistry: Principles and Commercial Applications*; Banks, R.E., Smart, B.E., Tatlow, J.C., Eds.; Plenum Press: New York, NY, USA, 1994; Chap. 3; pp. 57–88.
36. Krafft, M.P.; Riess, J.G. Selected physicochemical aspects of poly- and perfluoroalkylated substances relevant to performance, environment and sustainability-Part one. *Chemosphere* **2015**, *129*, 4–19. [[CrossRef](#)] [[PubMed](#)]
37. Chong, W.K.; Papadopoulou, V.; Dayton, P.A. Imaging with ultrasound contrast agents: Current status and future. *Abdom. Radiol.* **2018**, *43*, 762–772. [[CrossRef](#)] [[PubMed](#)]
38. Sirsi, S.; Borden, M. Microbubble compositions, properties and biomedical applications. *Bubble Sci. Eng. Technol.* **2009**, *1*, 3–17. [[CrossRef](#)] [[PubMed](#)]
39. Schutt, E.S.; Klein, D.H.; Mattrey, R.M.; Riess, J.G. Injectable microbubbles as contrast agents for diagnostic ultrasound imaging: The key role of perfluorochemicals. *Angew. Chem. Int. Ed.* **2003**, *42*, 3218–3235. [[CrossRef](#)]
40. Shibata, O.; Krafft, M.P. Mixed Langmuir monolayers made from single-chain perfluoroalkylated amphiphiles. *Langmuir* **2000**, *16*, 10281–10286. [[CrossRef](#)]
41. Krafft, M.P.; Goldmann, M. Monolayers made from fluorinated amphiphiles. *Curr. Opin. Colloid Interf. Sci.* **2003**, *8*, 243–250. [[CrossRef](#)]

Sample Availability: Samples of the compounds are not available from the authors.



© 2019 by the authors. Licensee MDPI, Basel, Switzerland. This article is an open access article distributed under the terms and conditions of the Creative Commons Attribution (CC BY) license (<http://creativecommons.org/licenses/by/4.0/>).